Superlattices and Microstructures 128 (2019) 265–273

Contents lists available at ScienceDirect

Superlattices and Microstructures

journal homepage: www.elsevier.com/locate/superlattices

Thermal transport in graphene field-effect transistors with ultrashort channel length

Mohamed Fadhel Ben Aissa[a,***], Houssem Rezgui[a,b,*], Faouzi Nasri[a,**], Hafedh Belmabrouk[c,d], AmenAllah Guizani[a,b]

[a] Laboratory of Thermal Processes, Research and Technology Centre of Energy, Hammam Lif, Tunisia
[b] University of Tunis El Manar, University Campus in Tunis, 2092, Manar II Tunis, Tunisia
[c] Laboratory of Electronics and Microelectronics, University of Monastir, Monastir, 5019, Tunisia
[d] Department of Physics, College of Science AlZulfi, Majmaah University, Al Majmaah, 11952, Saudi Arabia

ARTICLE INFO

Keywords:
Thermal transport
Thermal conductivity
Graphene field-effect transistor
Thermal stability
surface roughness
heat dissipation

ABSTRACT

Thermal management has been widely studied to enhance the reliability of future organic nanoelectronics. Organic Field-Effect Transistors (OFETs) represent a novel technology for future nanomanufacturing of electronic devices. However, enhancing the thermal stability of transistors become a major challenge for next-generation of electronics devices. In this work, we report the thermal transport of graphene FETs (GFETs) with ultrashort channel length. In the first step, we investigate the ability of our model to characterize the heat transport in nanotransistors. To clarify the nature of the phonon-wall collisions along the channel, we have considered the effect of the temperature jump boundary condition in the oxide-graphene interface. In addition, our proposed effective thermal conductivity (ETC) model agrees with experimental results. Furthermore, we have found that graphene FETs are more thermally stable than the classical transistors based on Silicon MOSFETs.

1. Introduction

In the past few years, Silicon (Si) was the most used semiconductor for microelectronics devices. However, Si-based devices are reaching their material limits due to the miniaturization [1]. With the rapid development of micro- and nano-fabrication in semiconductors, thermal stability in nanotransistors attracted researcher's attention due to their impact in the increasing of temperature in nanodevices [2,3]. Due to their excellent thermal properties, graphene transistors have been explored in order to find alternatives the Si technology. Graphene is the most useful carbon allotropes because of its ability in heat conduction. Graphene-based materials are involved in various applications such as flexible nanoelectronics [4], graphene field-effect transistors (GFETs) [5–10], light-emitting diodes (LEDs) [11] and solar cells [12].

In nanoscale devices, phonon transport should be investigated due to its importance in thermal conduction through nanoscale materials [13,14]. For Non-Fourier heat conduction, the thermal conductivity is reduced due to phonon scattering along the channel transistor, which implies the use of an effective thermal conductivity (ETC) [15–17]. Hua and Cao [15] have proposed an analytical solution from the Boltzmann transport equation (BTE) to model the ETC of ballistic-diffusive heat transport in nanofilms and

* Corresponding author. Laboratory of Thermal Processes, Research and Technology Centre of Energy, P.B N°95, 2050, Hammam Lif, Tunisia.
** Corresponding author.
*** Corresponding author.
E-mail addresses: fadbenai@yahoo.fr (M.F. Ben Aissa), houssem.rezgui@fst.utm.tn (H. Rezgui), nasrifaouzi90@yahoo.fr (F. Nasri).

https://doi.org/10.1016/j.spmi.2019.02.004
Received 12 November 2018; Received in revised form 16 January 2019; Accepted 8 February 2019
Available online 10 February 2019
0749-6036/

nanowires. Several previous papers have treated the size-dependent thermal conductivity in suspended single-layer graphene (SLG) and SiO_2-graphene [18–21]. It is found that the thermal conductivity depends on the specularity parameter p (probability of phonon scattering at the edge roughness). Under the BTE, the specularity p describes the thermal transport at the surface scattering where phonons scattering mechanism plays a key role in heat conduction [21]. Based on atomic force microscopy (AFM) measurements and scanning tunneling microscopy (STM) technique, we can clearly observe the topography of graphene on SiO_2 [22–25]. These techniques are used to study the surface properties and edge scattering in nanoscale materials.

Other similar works were carried out to evaluate the nanoscale heat transport in ballistic regime [26–30]. It is found that the ballistic regime appears with temperature jump at interface scattering as the Knudsen number (*Kn*) increases [29]. Nasri et al. [31] have investigated the performance of the single-phase lag model (SPL), where they have coupled the SPL model with the temperature jump boundary condition, to treat the heat transport in nanoscale silicon-on-insulator (SOI) metal-oxide semiconductor Filed-Effect Transistors (MOSFETs).

In this work, we use the BDE model related with a temperature jump boundary condition to characterize the phonon collisions and heat conduction process in nanotransistors. We take into account the Casimir limit estimated by the Ziman theory to predict the phonon scattering mechanism at the channel region [21]. To validate our prediction model, we have compared the thermal conductivity predicted by our theoretical model with computational studies [32,33] and experimental measurements of silicon thin-films at ambient temperature [34–36]. In addition, the good accordance with several surveys indicate the validity of our size dependence thermal conductivity of graphene on SiO_2 layer [18–20].

2. Computational model

Under the phonon BTE, the Gray relaxation-time approximation is given by Refs. [26–28,37]:

$$\frac{\partial f(r, v, t)}{\partial t} + v\nabla f(r, v, t) = -\frac{f - f_0}{\tau_R} \tag{1}$$

where f is the distribution function, f_0 is the equilibrium distribution, v is the group velocity, and τ_R is the relaxation time corresponding to resistive mechanisms defined as

$$\tau_R = \frac{3k}{Cv^2} \tag{2}$$

where C is the volumetric heat capacity and k is the thermal conductivity [28]. The ballistic-diffusive approach is obtained by separating the distribution function into two components $f = f_b + f_m$, where f_m is the diffusive part and f_b is the ballistic part which occurs from the boundary scattering [27]. The basic equation for the diffusive part f_m is expressed as:

$$\frac{\partial f_m(r, v, t)}{\partial t} + v\nabla f_m(r, v, t) = -\frac{f_m - f_0}{\tau_R} \tag{3}$$

In this way, we can calculate the diffusive heat flux [27]:

$$q_m(t, r) = \int_{\varepsilon} v(r, t) f_m(r, \varepsilon, t)\varepsilon D(\varepsilon) d\varepsilon \tag{4}$$

where ε is the kinetic energy and $D(\varepsilon)$ is the density of states. By applying the development in Taylor series to the first order of Eq. (3) and using the finite element method (FEM), we can obtain [14]:

$$\frac{f_m(r, \varepsilon(v), t + \tau_R) - f_m(r, \varepsilon(v), t)}{\tau_R} + v\nabla f_m(r, \varepsilon(v), t) = -\frac{f_m(r, \varepsilon(v), t) - f_0(r, \varepsilon(v))}{\tau_R} \tag{5}$$

By reorganizing the terms of Eq. (5), we can find

$$f_0(r, \varepsilon(v)) = \tau_R v\nabla f_m(r, \varepsilon(v), t) + f_m(r, \varepsilon(v), t + \tau_R) \tag{6}$$

Multiplying Eq. (6) with $\varepsilon D(\varepsilon)v$ and applying $\int_{\varepsilon} f_0 \varepsilon D(\varepsilon) v d\varepsilon = 0$, we can obtain

$$q_m(r, t + \tau_R) + \int_{\varepsilon} \tau_R v\nabla f_m(r, \varepsilon(v), t)\varepsilon D(\varepsilon) v d\varepsilon = 0 \tag{7}$$

Supposing that $\nabla f = \frac{df}{dT}\nabla T$, Eq. (7) becomes:

$$q_m(r, t + \tau_R) = -\kappa\nabla T_m(r, t) \tag{8}$$

where κ is the thermal conductivity defined as $\kappa = \int \tau_R v^2 \frac{df_m}{dT} \varepsilon D(\varepsilon) d\varepsilon$. Hence, the derivation of the previous equation leads to

$$\tau_R \frac{\partial q_m(r, t)}{\partial t} + q_m(r, t) = -\kappa\nabla T_m(r, t) \tag{9}$$

By using the same reasoning in Eq. (3), we can conclude that

$$\tau_R \frac{\partial q_b(r,\,t)}{\partial t} + q_b(r,\,t) = -\tau_R \times \nabla .\, q_b(r,\,t) \tag{10}$$

where $q_b$is the ballistic heat flux. Here, we take the divergence of Eq. (9) and by introducing the energy conservation equation, we obtain the original BDE model which, is given by the following expression

$$\tau_R \frac{\partial^2 T_m(r,\,t)}{\partial t^2} + \frac{\partial T_m(r,\,t)}{\partial t} = \frac{1}{C}\nabla(\kappa \nabla T_m(r,\,t)) - \frac{1}{C}\nabla q_b(r,\,t) + \frac{\dot{q}_h}{C} + \frac{\tau_R}{C}\frac{\partial \dot{q}_h}{\partial t} \tag{11}$$

where T_m is the temperature due to the diffusive components, $q_b$is the ballistic part of heat flux and $\dot{q}_h$is the volumetric heat generation.

In low thickness, smaller than the mean free path (MFP), phonon-rough-boundary scattering, affects the thermal transport. In some cases, phonons can travel ballistically from boundary to another one, which occurs in the confinement regime. In general, phonon confinements characterize the thermal transport at sub-10 nm size range [38]. This distribution generally named Casimir limit, which can be explained by the Ziman theory [21,29]. The size dependent thermal conductivity is modeled by solving the phonon BTE approach. Under the BTE, the thermal conductivity strongly varies with Knudsen number [17]. In this way, the size-dependent effective thermal conductivity along the channel transistor leads to the following expression [14,16,27]:

$$k_{eff}(Kn) = \kappa\left[1 - \frac{2Kn \times \tanh(1/2Kn)}{1 + C_w \times \tanh(1/2Kn)}\right] \tag{12}$$

where $Kn = \frac{\Lambda}{L_c}$is the Knudsen number, Λ is the phonon MFP and L_c is the characteristics channel length (distance between source and drain), $C_w = 2\left(\frac{1+p}{1-p}\right)$ is a constant associated to the properties of the material and $p$is the Ziman specularity parameter. This parameter is introduced to describe the phonon boundary collisions [27,30,38]. The regular expression for the specularity parameter is defined as:

$$p(\lambda) = \exp\left(-\frac{16\pi^3\eta^2}{\lambda^2}\right) \tag{13}$$

Where η is roughness coefficient and $\lambda$is the length of the incident phonon wave [21,38]. It is clear that the specularity increases when the root mean square decreases. The specularity parameter denotes to the quality of surface roughness. Higher specularity ($p > 0.5$) indicates that the surface is smooth and specular reflection takes place in the edge scattering. In this study, the suggested BDE model is calculated as [14,27]:

$$C\tau_b \frac{\partial^2 T_m(r,\,t)}{\partial t^2} + C\frac{\partial T_m(r,\,t)}{\partial t} = \kappa_{eff}\nabla\nabla T_m(r,\,t) - \nabla q_b(r,\,t) + \dot{q}_h + \tau_b \frac{\partial \dot{q}_h}{\partial t} \tag{14}$$

where τ_b is the relaxation time related to boundary scattering.

Under Eq. (14), a clear understanding of the size-dependent thermal conductivity, which obviously describes the interfacial heat transport across nanomaterials. By comparing Eq. (11) and Eq. (14), we show the difference between the original BDE and the present model. According to the proposed BDE model, the thermal transport is strongly influenced by the surface roughness.

In this paper, we emphasize on the impact of phonon-boundary collisions, which is frequent at low thickness. In this regard, we use of the Casimir-Ziman theory to describe the effect of phonon-surface scattering. Referring to Ziman theory, we can define the effective mean free path as [21,27]:

$$\Lambda_{eff} = v \times \tau_b \tag{15}$$

$$\Lambda_{eff} = L_c\frac{1+p}{1-p} \tag{16}$$

In order to take into account the phonon scattering phenomena in our structure especially in the oxide-graphene interface, we used a novel type of boundary condition given by Refs. [29,39,40]:

$$T - T_w = -d \times \Lambda \times \frac{\partial T}{\partial x} \tag{17}$$

where T_w is the wall temperature, $d$is a constant depending on the size of the used material. Alvarez and Jou [41] have clearly demonstrated that the heat transport depend on size of nanostructure and they have proposed a boundary condition written as [41]:

$$T - T_w = R \times q \tag{18}$$

where R is the thermal boundary resistance (TBR) and q is the heat flux. Sobolev [17] noted that the temperature jump appears due to the ballistic transport. Hence, the heat flux, can be written as:

$$q = -\kappa_{eff} \times \nabla T \tag{19}$$

The temperature jump boundary condition at X = 0 (oxide–graphene interface):

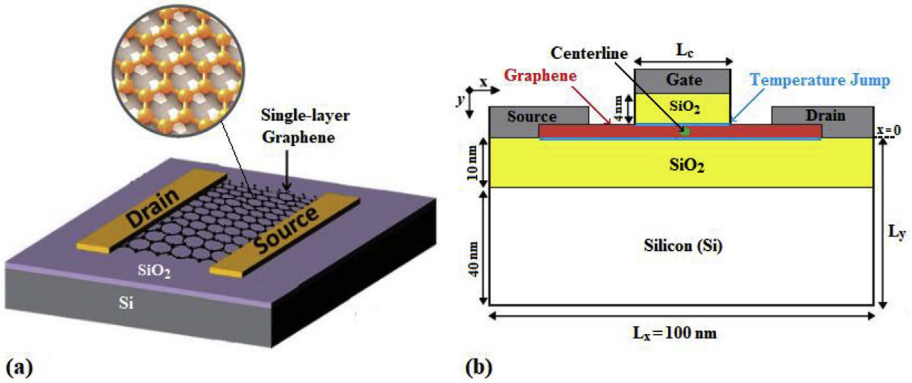

Fig. 1. (a) Schematic illustration of the device [10]. (b) Structure of graphene field-effect transistors (GFETs) [7].

$$T - T_w = -R \times \kappa_{eff} \times \left(\frac{\partial T}{\partial x}\right)_0 \tag{20}$$

By identification with Eq. (17), we obtain $d = \frac{R \times \kappa_{eff}}{Kn \times L_c}$ [39].

Recently, Rezgui et al. [14] have successfully validated the analytical approach for the temperature jump boundary condition. It was found that this boundary condition is an efficient method to treat the transient ballistic-diffusive heat transport within interfaces. In our suggested computational model, we assume that phonon-interface scattering dominates the phonon trajectory. By including the temperature jump boundary condition, we have introduced the acoustic confinement on the heat transport, which is due to the increase of phonon-boundary scattering. To enhance our present BDE model, we introduce the Ziman specularity parameter and the size-dependent effective thermal conductivity in order to get better predictions of the phonons-interface effects along the channel length. In addition, we took into account the thermal boundary resistance which describes the interfacial heat transport across nano-layers. Those rigorous modifications can improve the current BDE model for solving heat transfer across nano-layers. The main idea of this work is to understand the nature of heat dissipation, which is a significant challenge in future nanoelectronics.

3. Structures to model

Graphene transistors are considered as a state of the art technology due to their suitable thermal properties such as excellent thermal conductivity, good operating temperature and high electron mobility at ordinary temperature. Experimental results showed that electron mobility of GFETs varied from 10.000 to 15.000 cm^2Vs^{-1} [7]. As manufacturing nanodevices need higher performance, graphene transistors scaled to shorter channel length. In our simulation, we focus on the graphene FETs devices with 10 nm channel length [9]. Fig. 1(a) and Fig. 1(b), illustrate the geometry of the graphene FETs, which is extracted from the literature [7]. The proposed GFET structure consists of a single-layer graphene (SLG) integrated with SiO_2 top gate dielectric. Fig. 2(a) shows the atomic structure of graphene/SiO_2 interface, where the temperature jump boundary condition is applied.

Fig. 2(b) depicts the RMS roughness of graphene on SiO_2 layer. In this present work, we consider that the power generation rate is given by $\dot{q}_h = 110^{19} w/m^3$ and $T_{Ref} = 300$ K is the reference temperature. In order to compare the thermal stability of each nano-transistor the channel length of the (2D) Si FETs is $L_c = 10$ nm. For more details, the structure of the 2D conventional Si MOSFET is described in Refs. [27,31]. We keep the same length of L_x and L_y as denoted previously in Fig. 1(b). The characteristics of the used material are given in Table 1.

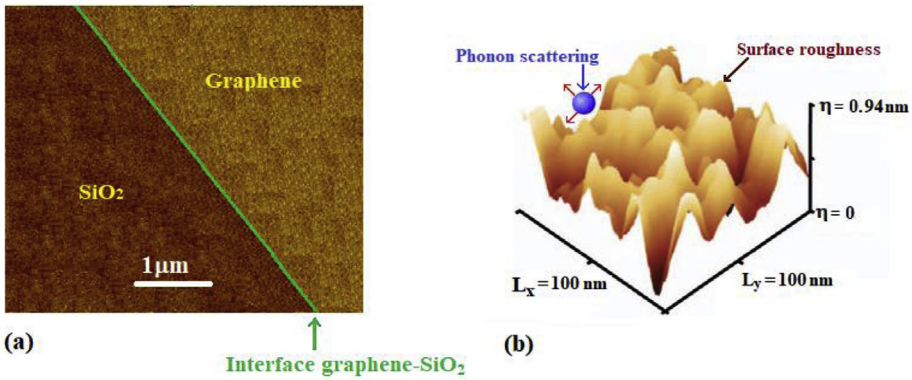

Fig. 2. (a) AFM image of topography of graphene-SiO_2 interface [22]. (b) STM topographic image of graphene on SiO_2 [25].

Table 1
Thermal properties of Silicon, graphene and Silicon dioxide.

Symbol	V (m s^{-1})	K (Wm^{-1} K^{-1})	C (J m^{-3} k^{-1})	Mean free path (nm)	References
Si	3000	150	1.5×10^6	100	[27]
Graphene	14740	4000	1.57×10^6	518	[27]
SiO_2	5900	1.4	1.75×10^6	0.4	[31]

4. Results and discussion

In this work, we report the heat transport by solving the ballistic-diffusive equation derived from the Boltzmann transport equation. According to Eq. (12), the ETC depends on the variation of Knudsen number. During our simulations, the heat transfer is predominated by the ballistic phonon transport because we focus on ultrashort channel transistor. The thickness of SLG is h = 0.335 nm, the mean free path is MFP_{Gr} = 518 nm and the ballistic scattering rate is $\frac{1}{\tau_b} = \left(\frac{1-p}{1+p}\right) \times \left(\frac{\nu}{L_c}\right)$ [27]. The MFP of suspended graphene is supposed to be in the order of 100–600 nm for a thermal conductivity ranged from 2000 to 4000 $Wm^{-1}K^{-1}$ [18]. To demonstrate the validity of the ETC model, we compare the obtained results with numerical and experimental results from the literature. Fig. 3 clarifies the relation of the thermal conductivity with the specularity parameter. We use the same values of phonon mean free path and bulk thermal conductivity in Ref. [33]. In low thickness (10 nm), the thermal conductivity achieves 15 $Wm^{-1}K^{-1}$. Yazdani et al. [33] found that the ETC ranging from 15 to 20 $Wm^{-1}K^{-1}$. Based on Raman spectra measurements, the effective thermal conductivity across the graphene-SiO_2 interface is estimated at K_{eff} = 600 $Wm^{-1}K^{-1}$ [20]. According to our proposed model, we find that K_{eff} = 592 $Wm^{-1}K^{-1}$ with p = 0.8 (smooth surface). For p = 0.5, the ETC is significantly reduced. Due to the utility of size-dependence effective thermal conductivity, additional data are summarized in Table 2.

To verify our proposed BDE model, we have compared our results with BTE, original BDE model [26] and the SPL model [31]. In this case, the thermal boundary resistance at Si/SiO_2 interface reaches 0.9 10^{-9} Km^2W^{-1} [42]. Fig. 4 depicts the comparison of the temporal distribution of the peak temperature rise in the centerline of the domain (x = L_x/2, y = 0) of the device. All models curves keep the same trend with different amplitude. Our proposed BDE curve with p = 0.5 is nearly to the SPL model and the classical BDE model. By using the new modification of the BDE model, it is clear that our suggested model estimates the increasing of the temperature better than the standard BDE model. With p = 0.25, the distribution of the temperature is near to the BTE model. The inclusion of the specularity, leads to a significant enhancement of the temperature profile because our proposed boundary condition describes the interfacial heat transport better than the SPL and the original BDE model. In addition, we show that the Fourier law cannot portend the phonon transport in nanostructure due to the infinite heat propagation speed.

Fig. 5 shows a comparison of the heat flux versus y-axis in the centerline (x = L_x/2) at t = 10 ps. It is found that the heat flux amplitude obtained in our model is close to the one obtained from BTE model. It is clear that the heat flux is maximum in the oxide-semiconductor interface due to the phonon-boundary scattering, which existed in this area. The heat flux depends on two essential parameters: (1) thickness of the heat zone and (2) type of phonon transport (diffusive or ballistic) [38]. In these conditions, p = 0.25 it is a good argument for non-Fourier heat transport.

In order to predict the thermal stability of each nano transistors, the specularity parameter is fixed at p = 0.8 for graphene FETs and p = 0.5 for Si MOSFETs. Experimental data's have demonstrated that the specularity parameter varied between 0.5 and 0.9 for graphene ribbons [43]. However, for silicon thin films the specularity was estimated at p = 0.25 to 0.5 when the RMS decreases from η = 1.63 nm to η = 0.54 nm [44]. The interface thermal resistance between graphene and SiO_2 is R = 4 10^{-8} Km^2W^{-1} [45]. In this

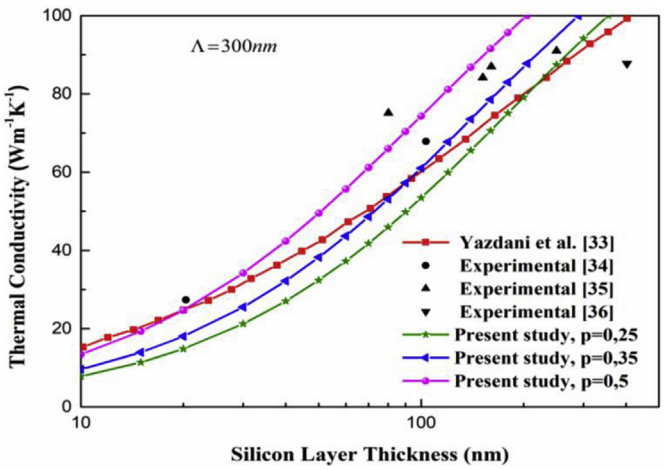

Fig. 3. Comparison of thermal conductivity for Silicon thin films at room temperature. Solid lines represent the theoretical model given by Eq. (12). The symbols denote the experimental results obtained in Refs. [34–36].

Table 2
Room temperature effective thermal conductivity of Graphene-SiO_2 interface and Silicon ultrathin films.

Sample	K ($Wm^{-1} K^{-1}$)	References
Graphene-SiO_2	600	[20]
Graphene-SiO_2	592	Present work (p = 0.8)
	219	Present work (p = 0.5)
Si (20 nm)	62 ($\Lambda = 40$ nm)	[32]
Si (10 nm)	15–20	Present work

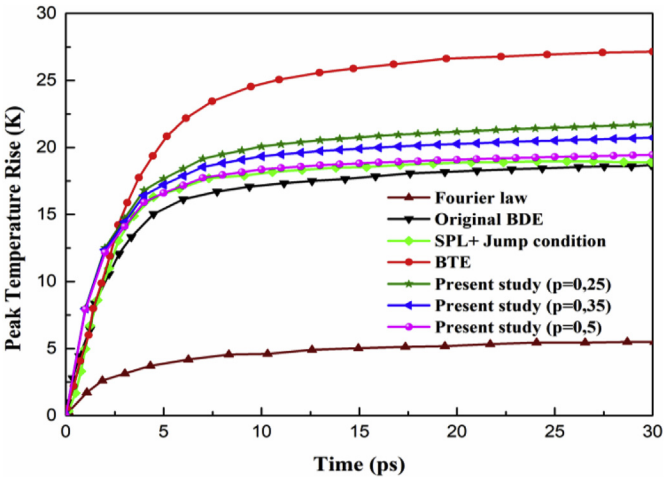

Fig. 4. Comparison of peak temperature along the centerline (X = $L_x/2$, Y = 0) of Si MOSFETs at t = 30 ps. Solid line and circles correspond to Boltzmann transport equation (BTE). Solid line and down triangles represent the original ballistic-diffusive equation (BDE) obtained in Ref. [26]. Solid line and diamond represent the single-phase lag model (SPL) associated with temperature jump boundary condition obtained in Ref. [31].

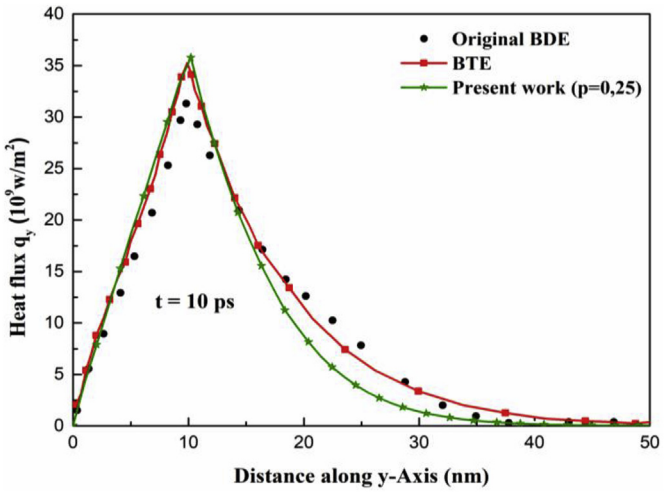

Fig. 5. Comparison of y-direction heat flux evolution of Si MOSFETs at t = 10 ps. Circles correspond to the original ballistic-diffusive equation (BDE). The solid line and squares correspond to Boltzmann transport equation (BTE) obtained in Ref. [26]. The solid line and stars represent the analytical solution of Eq. (19) with p = 0.25.

case, we compare the temperature and the heat flux evolution of each nanotransistor.

Fig. 6 illustrates a comparison of the temporal temperature in the centerline (x = $L_x/2$, y = 0) of the nanodevices at t = 60 ps. For Si and graphene FETs, the peak temperature reaches 322 K and 309 K respectively. It is clear that the graphene transistors are more thermally stable than Si transistors. Graphene material is implemented in electronic devices due to its excellent thermal conductivity and low consumption of energy [46]. These properties are making organic-based materials more suitable for nanomanufacturing and electronics cooling.

Fig. 7 represents the evolution of the temperature versus y-direction in the centerline (x = $L_x/2$) at different time. For the Si

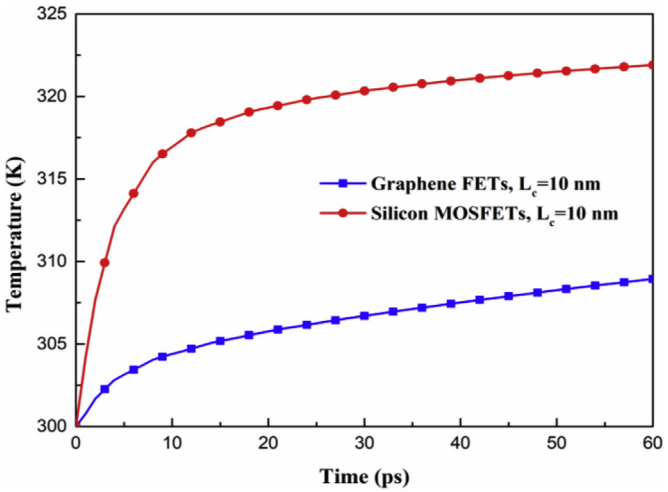

Fig. 6. Comparison of the temporal temperature profiles in graphene and silicon MOSFETs with 10 nm channel length at t = 60 ps. Solid line represents our proposed BDE model correspond to Eq. (14) coupled with the temperature boundary condition given by Eq. (17).

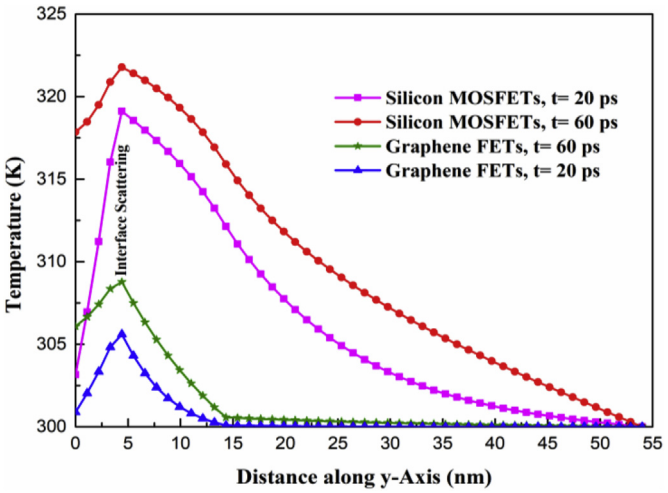

Fig. 7. Evolution of the peak temperature rise versus y-Axis in nanodevices at t = 20 and 60 ps.

MOSFETs the temperature is ranging from 319 K to 322 K. However, for the Graphene FETs the temperature varied from 305.6 K to 309 K. It is clear that the difference in the peak temperature appear for L = 4 nm (interface scattering). Due to the miniaturization of the device the collision rate $(1/\tau_b)$increases, it is the biggest cause of the self-heating in the nanodevices. The decrease of the thermal conductivity and the effects of phonons boundary scattering mechanisms cause the self-heating along the channel transistor. At the interface (oxide-semiconductor), the temperature jump occurs due to the collisions between the boundary and phonons [29,47].

Fig. 8 depicts the 2D heat flux distribution along y-direction in both devices at time scale t = 30 ps. It is obvious the heat flux is maximum in the interfacial contact between oxide (SiO2)-semiconductor. For the Si MOSFETs the heat flux reaches 14.7 (10^{10} W/m^2) and 86.2 (10^{10} W/m^2) for the Graphene transistors. Thus, Graphene FETs are favorable due to their high heat dissipation ability. In addition, graphene based transistors are designed to endure the increase of the heat dissipation due to its thermal conductivity, which is important for the safety of integrated circuits [48]. To enhance the thermal stability (reduce the temperature), it is necessary to increase the specularity parameter. Fig. 9 shows the impact of the specularity on the evolution of temperature along the y-direction of graphene FETs. Along the channel length, the thermal conductivity increases with the rise of the specularity, which, reduces the temperature rise of nanotransistor. Furthermore, GFETs have a smooth surface roughness (p > 0.5), which reduces the leakage current in nanodevices [11].

Graphene is an effective material in cooling devices and enhancing lifetime of electronics components. The performance of graphene-based devices leads to excellent thermal stability, which makes graphene FETs a good candidate to future transistor generation [49].

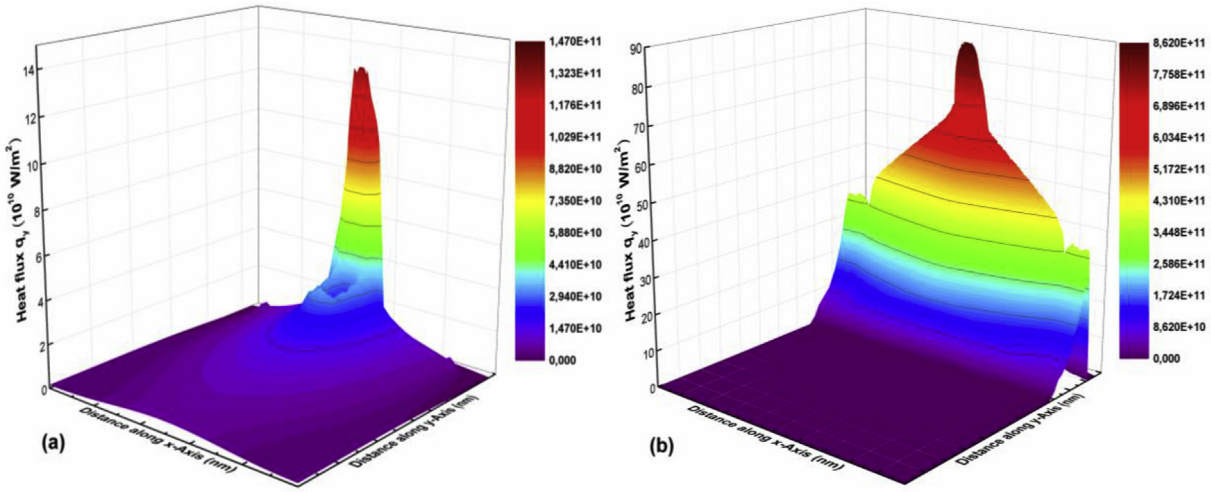

Fig. 8. 2D heat flux distribution at t = 30 ps for: (a) Si MOSFETs. (b) Graphene FETs.

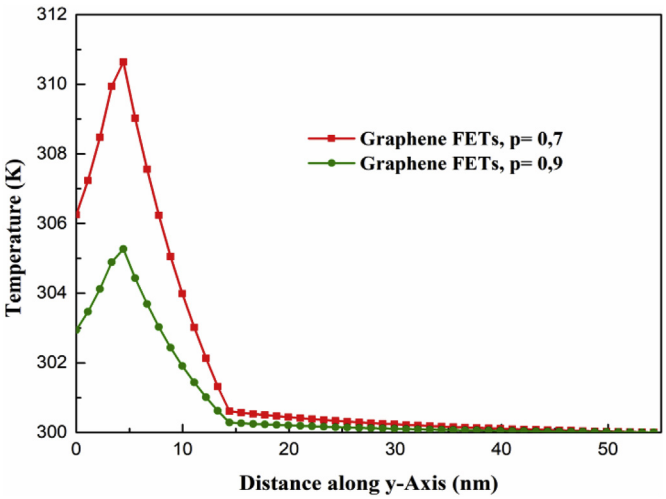

Fig. 9. Evolution of the peak temperature of graphene FETs along the line y at t = 50 ps for different values of specularity parameter.

5. Conclusion

In this work, we have investigated the thermal transport of graphene FETs with 10 nm channel length. To predict the thermal transport in GFET transistor, we have introduced the temperature jump boundary condition and the specularity parameter given by the Ziman theory. The validity of the proposed BDE model is verified by a comparison with other theoretical and experimental data extracted from the literature. Moreover, we found that the temperature jump occurs in the interface scattering due to the phonon-boundary scattering. Due to their low temperature and higher heat dissipation ability, graphene FETs are more thermally stable then Silicon MOSFETs. Due to the advantages of GFETs and the unique properties of graphene-based materials, organic transistors would give more opportunities for new devices in the next generation electronics. In the next future, we will report the thermal stability of thin-films transistors based on graphene on h-BN heterostructures [50].

Appendix A. Supplementary data

Supplementary data to this article can be found online at https://doi.org/10.1016/j.spmi.2019.02.004.

References

[1] F. Nasri, F. Echouchene, M.F. Ben Aissa, I. Graur, H. Belmabrouk, Investigation of self-heating effects in a 10-nm SOI-MOSFET with an insulator region using electrothermal modeling, IEEE Trans. Electron Devices (62) (2015) 2410–2415.
[2] A. Reuveny, T. Yokota, R. Shidachi, T. Sekitani, T. Someya, Thermal stability of organic transistor with short channel length on ultrathin foils, Org. Electron. 26

(2015) 279–284.
[3] M.H. Bae, Z.Y. Ong, D. Estrada, E. Pop, Imaging, simulation, and electrostatic control of power dissipation in graphene devices, Nano Lett. 10 (2010) 4787–4793.
[4] D. Akinwande, N. Petrone, J. Hone, Two-dimensional flexible nanoelectronics, Nat. Commun. 5 (5678) (2014).
[5] A. Sotoudeh, M. Amirmazlaghani, Graphene-based field effect diode, Superlattice. Microst. 120 (2018) 828–836.
[6] G. Fiori, F. Bonaccorso, G. Iannaccone, T. Palacios, D. Neumaier, A. Seabaugh, S.K. Banerjee, L. Colombo, Electronics based on two-dimensional materials, nature nanotech 9 (2014) 768–779.
[7] F. Schwierz, Graphene transistors, Nat. Nanotechnol. 5 (2010) 487–496.
[8] K. Kim, J.Y. Choi, T. Kim, S.H. Cho, H.J. Chung, A role for graphene in silicon-based semiconductor devices, Nature 479 (2011) 338–344.
[9] J. Zheng, L. Wang, R. Quhe, Q. Liu, H. Li, D. Yu, W.N. Mei, J. Shi, Z. Gao, J. Lu, Sub-10 nm gate length graphene transistors: operating at terahertz frequencies with current saturation, Sci. Rep. 3 (2013) 1314.
[10] M. Eslamian, Inorganic and organic solution-processed thin film devices, Nano-Micro Lett. 9 (3) (2017).
[11] T.H. Han, H. Kim, S.J. Kwon, T.W. Lee, Graphene-based flexible electronic devices, Mater. Sci. Eng. R 118 (2017) 1–43.
[12] X. Zhang, Y. Zhang, Z. Ye, W. Li, T. Liao, J. Chen, Graphene-based thermionic solar cells, IEEE Electron. Device Lett. 39 (2018) 383–385.
[13] N. Lu, L. Li, N. Gao, M. Liu, A unified description of thermal transport performance in disorder organic semiconductors, Org. Electron. 41 (2017) 294–300.
[14] H. Rezgui, F. Nasri, M.F. Ben Aissa, F. Blaabjerg, H. Belmabrouk, A.A. Guizani, Investigation of heat transport across Ge/Si interface using an enhanced ballistic-diffusive model, Superlattice. Microst. 124 (2018) 218–230.
[15] Y.C. Hua, B.Y. Cao, The effective thermal conductivity of ballistic-diffusive heat conduction in nanostructures with internal heat source, Int. J. Heat Mass Transf. 92 (2016) 995–1003.
[16] A. Sellito, l. Carlomango, D. Jou, Two-dimensional phonon hydrodynamics in narrow strips, Philos. Trans. Roy. Soc. London A, Math. Phys. Sci. 471 (2015) 2182.
[17] S.L. Sobolev, Discrete space-time model for heat conduction: application to size dependent thermal conductivity in nano-films, Int. J. Heat Mass Transf. 108 (2017) 933–939.
[18] E. Pop, V. Varshney, A.K. Roy, Thermal properties of graphene: fundamentals and applications, MRS Bull. 37 (2012) 1273–1281.
[19] M.H. Bae, Z. Li, Z. Aksamija, P.N. Martin, F. Xiong, Z.Y. Ong, I. Knezevic, E. Pop, Ballistic to diffusive crossover of heat flow in graphene ribbons, Nat. Commun. 4 (2013) 1734.
[20] J.H. Seol, I. Jo, A.L. Moore, L. Lindsay, Z.H. Aitken, M.T. Pettes, X. Li, Z. Yao, R. Huang, D. Broido, N. Mingo, R.S. Ruoff, L. Shi, Two-dimensional phonon transport in supported graphene, Science 328 (2010) 213–216.
[21] J.B. Hertzberg, M. Aksit, O.O. Otelaja, D.A. Stewart, R.D. Robinson, Direct measurements of surface scattering in Si nanosheets using a microscale phonon spectrometer: implication for Casimir-limit, Nano Lett. 14 (2) (2014) 403–415.
[22] J.S. Choi, J.S. Kim, I.S. Byum, D.H. Lee, M.J. Lee, B.H. Park, C. Lee, D. Yoon, H. Cheong, K.H. Lee, Y.W. Son, J.Y. Park, M. Salmeron, Friction anisotropy-driven domain imaging on exfoliated monolayer graphene, Science 333 (2011) 607–610.
[23] S.R. Pathipati, E. Pavlica, K. Parvez, X. Feng, K. Mullen, G. Bratina, Graphene flakes at the SiO_2/organic-semiconductor interface for high-mobility field-effect transistors, Org. Electron. 27 (2015) 221–226.
[24] M. Yankowitz, J. Xue, B.J. Leroy, Graphene on hexagonal boron nitride, J. Phys. Condens. Matter 26 (2014) 303201.
[25] J. Xue, J. Sanchez-Yamagishi, D. Bulmash, P. Jacquod, A. Deshpande, K. Watanbe, T. Taniguchi, P. Jarillo-Herrero, B.J. Leroy, Scanning tunneling microscopy and spectroscopy of ultra-flat graphene on hexagonal boron nitride, Nat. Mater. 10 (2011) 282–285.
[26] R. Yang, G. Chen, M. Laroche, Y. Taur, Simulation of nanoscale multidimensional transient heat conduction problems using ballistic-diffusive equations and phonon Boltzmann equation, ASME J. Heat Transf. 127 (2005) 298–306.
[27] H. Rezgui, F. Nasri, M.F. Ben Aissa, H. Belmabrouk, A.A. Guizani, Modeling thermal performance of nano-GNRFET transistor using ballistic-diffusive equation, IEEE Trans. Electron Devices 65 (4) (2018) 1611–1616.
[28] Y. Zhang, W. Ye, Modified ballistic-diffusive equations for transient non-continuum heat condition, Int. J. Heat Mass Transf. 83 (2015) 51–63.
[29] Y.C. Hua, B.Y. Cao, Slip boundary conditions in ballistic-diffusive heat transport in nanostructures, Nanoscale Microscale Thermophys. Eng. 21 (3) (2017) 159–176.
[30] R. Anufriev, A. Ramiere, J. Maire, M. Nomura, Heat guiding and focusing using ballistic phonon transport in photonic nanostructures, Nat. Commun. 8 (15505) (2017).
[31] F. Nasri, M.F. Ben Aissa, M.H. Gazzah, H. Belmabrouk, 3D thermal conduction in nanoscale Tri-Gate MOSFET based on single-phase-lag model, Appl. Therm. Eng. 91 (2015) 647–653.
[32] Y. Guo, M. Wang, Phonon hydrodynamics and its applications in nanoscale heat transport, Phys. Rep. 595 (2015) 1–44.
[33] K.E. Yazdani, Y. Yang, M. Asheghi, Ballistic phonon transport and self-heating effects in strained-silicon transistors, IEEE Trans. Compon. Packag. Technol. 29 (2006) 254–260.
[34] M. Asheghi, M.N. Touzelbaev, K.E. Goodson, Y.K. Leung, S.S. Wong, Temperature depend thermal conductivity of single-crystal silicon layers in SOI substrates, ASME J. Heat Trans. 120 (1998) 30–36.
[35] Y.S. Ju, K.E. Goodson, Phonons scattering in silicon films thickness of order 100 nm, Appl. Phys. Lett. 74 (1999) 3005–3007.
[36] W. Liu, M. Asheghi, Phonon boundary scattering in ultra-thin single crystal silicon layers, Appl. Phys. Lett. 84 (2004) 3819–3821.
[37] S.L. Sobolev, Hyperbolic heat conduction, effective temperature, and third law for nonequilibrium systems with heat flux, Phys. Rev. E 97 (2018) 022122.
[38] S. Kwon, M.C. Wingert, J. Zheng, J. Xiang, R. Chen, Thermal transport in Si and Ge nanostructures in the 'confinement' regime, Nanoscale 8 (27) (2016) 13155–13167.
[39] M.F. Ben Aissa, F. Nasri, H. Belmabrouk, Multidimensional nano heat conduction in cylindrical transistors, IEEE Trans. Electron Devices 64 (12) (2017) 5236–5241.
[40] A. Cheng, S. Chen, H. Zeng, D. Ding, R. Chen, Transient analysis for electrothermal properties in nanoscale transistors, IEEE Trans. Electron Devices 65 (9) (2018) 3930–3935.
[41] F.X. Alvarez, D. Jou, Boundary conditions and evolution of ballistic heat transport, J. Heat Tran. 132 (2010) 012404.
[42] J. Chen, G. Zhang, B. Li, Thermal contact resistance across nanoscale silicon dioxide and silicon interface, Appl. Phys. Lett. 112 (2012) 064319.
[43] D.L. Nika, A.S. Askerov, A.A. Balandin, Anomalous size dependence of the thermal conductivity of graphene ribbons, Nano Lett. 12 (6) (2012) 3238–3244.
[44] X. Wang, B. Huang, Computational study of in-plane phonon transport in Si thin films, Sci. Rep. 4 (2014) 6399.
[45] K.M.F. Shail, A.A. Balandin, Thermal properties of graphene and multilayer graphene: applications in thermal interface materials, Solid State Commun. 152 (2012) 1331–1340.
[46] M. Irimia-Vladu, Green electronics: biodegradable and biocompatible materials and devices for sustainable future, Chem. Soc. Rev. 43 (2014) 588–610.
[47] F. Nasri, M.F. Ben Aissa, H. Belmabrouk, Nonlinear electrothermal model for investigation of heat transfer process in a 22-nm FD-SOI MOSFET, IEEE Trans. Electron Devices 64 (2017) 1461–1466.
[48] H. Zhang, H. Wang, S. Xiong, H. Han, S. Volz, Y. Ni, Multi-Scale modeling of heat dissipation in 2D transistors based on phosphorene and silicene, J. Phys. Chem. C 122 (2018) 2641–2647.
[49] F. Schwierz, J. Pezoldt, R. Granzner, Two-dimensional materials and their prospects in transistor electronics, Nanoscale 7 (2015) 8261–8283.
[50] M. Souibgui, H. Ajlani, A. Cavanna, M. Oueslati, A. Meftah, A. Madouri, Raman study of annealed two-dimensional heterostructure of graphene on hexagonal boron nitride, Superlattice. Microst. 112 (2017) 394–403.